Contrib Mineral Petrol (1992) 110:33–45

Contributions to Mineralogy and Petrology

Nd-, Sr-, O-isotopic and chemical evidence for a two-stage contamination history of mantle magma in the Central-Alpine Bergell intrusion

Friedhelm von Blanckenburg [1,*], Gretchen Früh-Green [2], Karlheinz Diethelm [2], and Peter Stille [1,]**

[1] Institut für Kristallographie und Petrographie, ETH-Zentrum, CH-8092 Zürich, Switzerland
[2] Institut für Mineralogie und Petrographie, ETH-Zentrum, CH-8092 Zürich, Switzerland

Received December 5, 1990 / Accepted September 2, 1991

Abstract. Two different contamination processes have been identified as having been operative in the genesis of a plutonic suite: initial contamination of a mantle source, and subsequent crustal contamination of uprising partial melts from the mantle. These processes are indicated by a detailed analyses of Nd, Sr, and oxygen isotopes together with major- and trace-elements of the 32–30 Ma calc-alkaline Bergell intrusion. This intrusion is located at the suture of the Alpine continental collision zone and contains rock types capable of discriminating between mantle and intracrustal processes. A range from basaltic-andesitic dykes in the surrounding country rocks, cumulitic hornblendites, gabbros, tonalite, granodiorite and lamprophyres, to pegmatites and aplites, is exposed in this single intrusion. The results of REE modelling and isotopic compositions of the basic members suggest that the cumulates were fractionated from a picrobasaltic liquid originating by partial melting of enriched subcontinental mantle ($\varepsilon_{Nd} = +4$). Increases in $^{87}Sr/^{86}Sr$ (0.7055) and $\delta^{18}O$ (+6.7) in these samples relative to the mantle array and compositions of other Periadriatic intrusions are most likely the result of an initial contamination of the mantle source by dehydration or partial melting of altered subducted oceanic crust. Slight differentiation of such a picrobasaltic liquid produced the basaltic-andesitic dykes. Simultaneous fractional crystallization and contamination of the uprising magma by continental crust produced crustal isotopic signatures which increase with acidity to values of $\varepsilon_{Nd} = -7.6$, $^{87}Sr/^{86}Sr = 0.716$ and $\delta^{18}O = +10$. The crustal imprint and LREE enrichment in the dominating tonalite increase with decreasing crystallization depth which indicates that the tonalites were emplaced in several distinct batches with different degrees of contamination. Shoshonitic lamprophyres, which intruded into the partly solidified granodiorite, were generated in a deep, strongly contaminated mantle source. The posttectonic 26 Ma Novate leucogranite is not cogenetic with the main Bergell body, but rather formed from a predominantly crustal source. If the described features are indeed due to mantle source contamination processes, which are well known for volcanic arcs, it must be concluded that these may also play a significant role in the genesis of calc-alkaline plutonic suites.

Present adresses:
* Department of Earth Sciences, University of Cambridge, Downing Street, Cambridge CB2 3EQ, UK
** Centre de Geochimie de la Surface, C.N.R.S., 1, rue Blessig, F-67000 Strasbourg-Cedex, France

Offprint requests to: F. von Blanckenburg

Introduction

The thorough isotopic and geochemical analysis of all members of a *single* igneous complex offers an excellent opportunity to study both the sources which contributed to the pluton and the processes involved in its genesis. In general, crustal contamination increases with the degree of differentiation. As a consequence the study of basic members of an intrusion is particularly valuable for observing mantle processes, whereas the acidic components may yield information on intracrustal processes. Taylor (1980) and DePaolo (1981) have quantified this "assimilation and fractional crystallization (AFC)" process.

Another mechanism often encountered in calc-alkaline, and thus continental margin magmatism, is the "source contamination" process (James 1981), where the mantle source of the magmas is contaminated by subducted materials. This process, however, is difficult to identify by major or trace element geochemistry in plutonic rocks because all intrusive members and thus their elemental concentrations are usually modified by fractional crystallization. Nevertheless a combination of sensitive isotopic indicators, such as Sr and Nd, which have high contaminant/mantle concentration ratios, with an abundant element such as oxygen with approximately equal concentrations in mantle and contaminant, often enables a distinction to be made between source contamination and other processes (James 1981). Source

contamination has often been observed in island arcs (Davidson and Harmon 1989; Chen et al. 1990; for two recent examples and references therein) and continental volcanic arcs (Stern et al. 1990), but only rarely in plutonic arcs (Hill et al. 1986).

This paper focusses on the identification of the different sources of a single pluton, the 32–30 Ma Central Alpine Bergell intrusion. Major and trace element geochemical, oxygen-, Sr-, and Nd-isotopic analyses are presented for all major rock types ranging from cumulitic hornblendite to pegmatite. The Bergell intrusion is located at the triple point of the Eastern, Southern and Central Alps, aligned like several other Tertiary intrusions along the late Alpine "Periadriatic" (Insubric) fault system and is most certainly linked to deep reaching lithospheric processes in the Alps. An understanding of the origin of this intrusion is thus of fundamental significance.

Geological Framework

The Bergell intrusion is located in the southeast corner of the zone of Tertiary ("Lepontine") metamorphism. The massif consists mainly of a zoned structure made up of mafic dykes in the country rocks, marginal occurrences of cumulates and gabbros, a frame of tonalite ("serizzo" in Italian) and a granodiorite ("ghiandone") centre (Fig. 1). A separate peraluminous intrusion, the Novate leucogranite, crosscuts both tonalite and granodiorite, is undeformed, and according to trace element variations, unrelated to the main Bergell body (Gulson 1973; Reusser 1987).

The three main units have been dated by the U–Pb method: the tonalite yields discordant zircon ages >30 Ma, the granodiorite both discordant zircon and a concordant accessory mineral age at 30 Ma (Gulson and Krogh 1973), and the Novate leucogranite a concordant monazite age of 26 Ma (Köppel and Grünenfelder 1975). Von Blanckenburg (1990) investigated the Sm–Nd and U–Th–Pb systematics of accessory minerals and determined precise intrusion ages of 31.89 ± 0.09 Ma by zircons from the tonalite and 30.1 ± 0.17 Ma by allanite and sphene from the granodiorite.

Geological maps have been published by Staub (1921) and Wenk and Cornelius (1977), and a geological summary on the Bergell intrusion and its field relations is given by Trommsdorff and Nievergelt (1983).

The following rock types have been investigated and are discussed in the sequence of emplacement: Basaltic-andesitic dykes, which crosscut the regional metamorphic and folded country rocks in the north and southeast of the intrusion (Nievergelt and Dietrich 1977; Gautschi and Montrasio 1978) represent the first phase of magmatism in the region, as some of them are overprinted by contact metamorphism within the Bergell contact aureole. Cumulitic hornblendites and gabbros are the first members of the intrusion itself and have been carried up from a depth of ~ 30 km to the margins of the massif as large solid blocks by the subsequent acidic intrusions (Diethelm 1985, 1989). Only gabbros from the comparatively larger mafic bodies of the eastern margin were studied in order to avoid the metasomatic overprint on the small gabbro lenses of the western margin. The tonalite is hornblende-rich and extends over 60 km toward the west in an offshoot called the "Iorio tonalite" (Weber 1957). Reusser (1987) suggested an increase in hornblende crystallisation pressure from 5 kbar in the east to 7.5 kbar in the west based on hornblende barometry. The tonalite becomes increasingly foliated from east to west. Small occurrences of in situ crystallized gabbros and microgabbros were emplaced simultaneously with the tonalite at the present level of exposure and contain restitic material of undissolved country rocks. The granodiorite, the largest unit of the intrusion, contains large alkalifeldspar crystals and is in part hornblende bearing. Lamprophyres intruded the partly solidified granodiorite. In part they are disintegrated into xenoliths. Both calc-alkaline and shoshonitic dykes exist (Diethelm 1989). For the present study a shoshonitic lamprophyre was analyzed. The "Melirolo Augengneis" (Weber 1957) is a small strongly foliated plagioclase augen bearing granodiorite, which forms the southern margin of the Iorio tonalite. Both aplites and pegmatites crosscut the older intrusions and country rocks discordantly, and form the final members of the intrusion. A roof pendant was analyzed from the pre-Alpine Suretta nappe, which rests in the east as a large body on the granodiorite and represents a typical, though not representative potential crustal contaminant.

The genesis of the Bergell intrusion has long been subject to debate. In general, two models have been proposed to account for its origin. (a) The in situ transformation of country rock (Drescher-Kaden 1940; Wenk and Cornelius 1977; Wenk 1982). This model basically proposed a subsolidus metasomatic mixing of amphibolitic and granitic country rock to form gabbros and the tonalite. (b) The Bergell as intrusive massif: Staub (1918) interpreted the massif as a postkinematic magmatic intrusion. This idea was supported among others by Clondiffe and Mottana (1974), who performed melting experiments on granodiorite and tonalite, Trommsdorff and Nievergelt (1983) by field observations, Diethelm (1985), who demonstrated the intrusive character of the Bergell

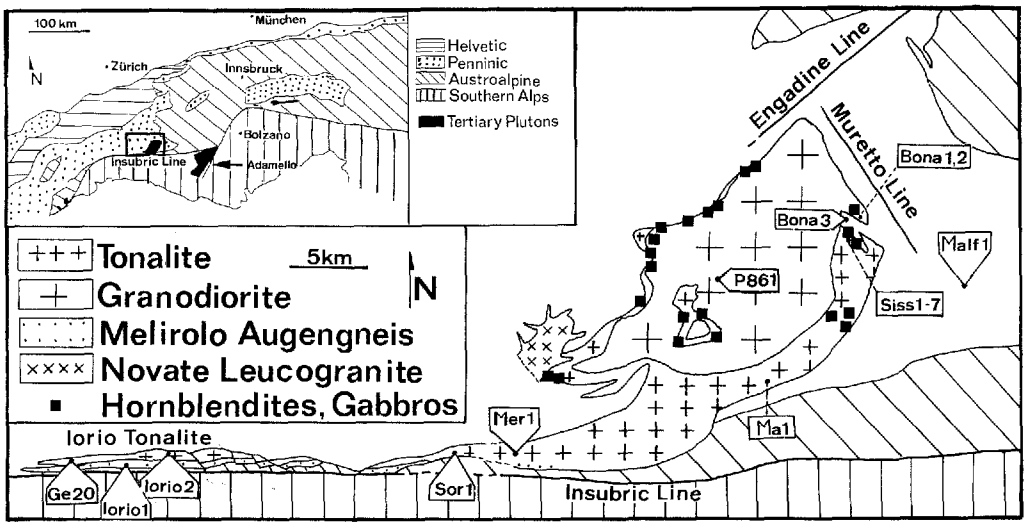

Fig. 1. Simplified geological map of the Bergell intrusion showing the principal rock types and sample locations. After Weber (1957), Trommsdorff and Nievergelt (1983), and Diethelm (1989)

Table 1. Major- and trace-element concentrations. All measurements by XRF except for INAA [a], and isotope dilution [b]. n.d. = not determined. Samples are sorted in order of geological appearance, tonalites from east to west

	Malf1 Basalt	Siss4 Hbldt	Siss6 Hbldt	Siss1 Gabbro	Siss2 Gabbro	Siss3 Tona	Ma1 Tona	Mer1 Tona	Sor1 Tona	Iorio2 Tona	Ge20 Tona	Bona1 Grdt	P861 Shosh	Iorio1 Mel AG	Bona2 Aplite	Siss7 Pegma	Bona3 Roof Pcn
Major Elements (weight %)																	
SiO_2	49.87	46.92	45.92	47.95	48.81	57.64	57.25	56.43	55.61	54.89	57.93	66.30	51.11	62.39	73.76	75.57	70.67
TiO_2	1.08	0.63	0.58	0.72	1.04	0.68	0.75	0.73	0.77	0.74	0.69	0.37	0.94	0.57	0.11	0.05	0.43
Al_2O_3	18.71	7.54	6.08	7.57	15.64	16.82	17.62	17.42	17.58	18.40	17.36	15.50	12.34	17.30	14.55	14.29	14.73
Fe_2O_3	9.07	3.22	2.81	1.62	1.68	2.17	7.33	2.42	2.54	2.39	1.81	0.66	1.15	1.28	0.37	0.27	1.17
FeO	n.d.	5.80	8.15	5.30	7.05	4.05	n.d.	4.60	4.80	4.70	4.55	2.15	5.25	2.90	0.60	0.25	1.90
MnO	0.16	0.15	0.20	0.15	0.13	0.10	0.13	0.14	0.14	0.12	0.11	0.04	0.15	0.06	0.04	0.00	0.06
MgO	5.13	16.51	20.49	13.26	8.90	3.66	3.84	4.21	4.36	4.21	3.79	1.68	10.11	2.27	0.26	0.12	0.97
CaO	9.56	15.94	13.34	17.66	10.54	6.69	7.56	7.89	8.08	8.18	7.42	3.09	8.23	5.21	1.01	0.84	2.49
Na_2O	5.45	0.71	0.56	0.95	1.71	3.06	3.11	3.12	2.89	3.08	3.10	3.37	1.60	3.14	4.42	3.82	3.48
K_2O	0.25	0.15	0.14	0.20	1.16	2.18	1.72	1.73	1.71	1.32	1.67	4.41	5.08	2.67	4.63	4.28	3.58
P_2O_5	0.15	0.05	0.03	0.06	0.12	0.22	0.19	0.22	0.23	0.17	0.16	0.26	0.76	0.20	0.10	0.07	0.12
H_2O	n.d.	1.83	1.32	3.46	2.06	1.40	n.d.	0.98	1.24	1.34	1.14	0.71	0.75	0.96	0.26	0.47	0.68
Total	99.43	99.45	99.62	98.90	98.84	98.67	99.50	99.89	99.95	99.54	99.73	98.54	97.47	98.95	100.11	100.03	100.28
Trace-Elements (ppm)																	
F	<50	255	378	564	723	636	482	506	709	519	504	723	1476	560	196	304	469
Ba	92	20	33	28	168	556	446	461	457	203	301	852	1712	407	201	94	741
Rb[b]	2.393	7.908	4.077	5.048	58.95	91.36	64.43	67.44	65.10	45.46	64.49	199.5	251.3	98.41	250.0	178.1	104.1
Sr[b]	326.9	65.21	54.74	77.67	248.6	320.1	299.7	353.0	362.8	290.8	240.9	346.4	626.2	250.6	86.44	48.38	219.4
Y	19	<2	7	<2	23	18	22	17	24	12	14	4	12	17	<2	10	7
Zr	74	11	20	21	65	131	137	99	129	81	104	129	205	138	50	17	145
V	331	290	252	316	312	181	215	219	236	218	195	70	191	110	<10	<10	53
Cr	6	998	314	348	99	18	20	21	21	<6	11	21	536	15	<6	<6	<6
Ni	20	204	149	68	33	<3	13	17	16	<3	<3	<3	163	<3	<3	<3	<3
Co	54	75	127	47	28	<3	31	20	40	8	3	12	19	12	26	23	21
Cu	<3	86	29	8	<3	<3	17	16	17	23	21	<3	<3	<3	<3	<3	<3
Zn	53	44	64	41	74	63	71	72	78	66	61	39	74	47	28	14	48
Sc	39	89	101	117	63	25	31	28	31	27	28	9	29	8	2	3	6
S	<50	240	73	<50	<50	<50	<50	<50	<50	<50	<50	<50	<50	<50	<50	<50	<50
Th[a]	1.9	<0.5	<0.5	1.0	1.3	10.93[b]	5.4	7.6	9.9	4.0	1.4	18.81[b]	18.4	8.9	5.6	6.5	11.4
U[a]	0.6	<0.1	<0.1	0.3	<0.1	2.34[b]	1.6	2.8	2.6	0.8	0.9	11.85[b]	6.8	1.5	4.6	7.00	1.1
Hf[a]	2.3	0.9	1.0	1.3	2.6	4.8	3.8	2.4	3.6	2.6	3.9	4.8	6.5	4.5	2.3	1.3	4.1
La[a]	6.7	1.1	1.5	2.8	9.5	28.5	21.9	14.3	24.2	20.8	11.1	32.9	59.2	30.2	8.7	4.5	34.0
Ce[a]	17.0	3.6	3.6	6.4	25.6	59.7	48.9	29.4	53.4	36.2	27.3	63.3	117	61.7	16.5	8.6	61.5
Nd[b]	12.76	3.939	4.363	6.270	22.55	26.66	25.19	20.55	27.83	18.41	16.83	23.97	50.89	25.91	8.874	6.383	31.63
Sm[b]	3.674	1.444	1.552	2.082	6.025	5.734	5.616	4.494	6.229	4.073	3.945	4.624	8.690	5.407	1.993	1.848	5.297
Eu[a]	1.3	0.4	0.4	0.5	1.1	1.2	1.2	0.9	1.3	1.1	0.9	1.0	2.0	1.1	0.2	0.2	0.8
Tb[a]	0.6	0.3	0.3	0.3	0.7	0.8	0.8	0.5	0.9	0.7	0.6	0.6	1.0	0.8	0.3	0.3	0.4
Yb[a]	2.8	0.8	0.9	1.3	2.5	2.8	2.9	1.6	2.9	2.2	2.4	1.5	1.9	2.5	0.9	1.7	0.8
Lu[a]	0.4	0.2	0.1	0.2	0.4	0.5	0.4	0.2	0.4	0.4	0.4	0.2	0.3	0.4	0.1	0.2	0.1

Table 2. Isotope dilution data and isotopic ratios. Samples are sorted in order of geological appearance, tonalites from east to west. A $^{87}Rb/^{86}Sr$-error of 0.6% was propagated into time-corrected $^{87}Sr/^{86}Sr$ ratios. All uncertainties given are for the 95% C.L. except for $\delta^{18}O$, for which one standard deviation of multiple measurements is given. The number of $\delta^{18}O$ measurements is given in parentheses

Sample	Rb [ppm]	Sr [ppm]	$^{87}Rb/^{86}Sr$	$^{87}Sr/^{86}Sr$ [measured]	$^{87}Sr/^{86}Sr$ [30 Ma]	ε_{Sr} [30 Ma]	Sm [ppm]	Nd [ppm]	$^{147}Sm/^{144}Nd$	$^{143}Nd/^{144}Nd$ [measured]	ε_{Nd} [0]	ε_{Nd} [30 Ma]	$\delta^{18}O$(#)
Basaltic Dyke													
Malf 1	2.393	326.9	0.02117	0.705656 50	0.705647 50	16.78 71	3.674	12.76	0.1741	0.512841 7	+3.95 14	+4.05 14	6.71 11(5)
Cumulitic Hornblendites and Hornblende Gabbros													
Siss 4	7.908	65.21	0.3508	0.705679 37	0.705530 38	15.12 54	1.444	3.939	0.2215	0.512760 25	+2.39 49	+2.29 49	6.72 26(6)
Siss 6	4.077	54.74	0.2154	0.706189 23	0.706097 24	23.17 34	1.552	4.363	0.2150	0.512704 9	+1.28 18	+1.22 18	6.85 18(5)
Siss 1	5.048	77.67	0.1880	0.707144 28	0.707064 29	36.90 41	2.082	6.270	0.2007	0.512660 23	+0.43 45	+0.41 45	7.07 08(4)
In-situ crystallized Gabbro													
Siss 2	58.95	248.6	0.6862	0.709800 49	0.709508 53	71.58 75	6.025	22.55	0.1615	0.512324 9	−6.13 18	−5.99 18	8.65 54(4)
Tonalites (from E to W)													
Siss 3	91.36	320.1	0.8261	0.710353 91	0.710001 94	78.6 1.3	5.734	26.66	0.1300	0.512378 5	−5.07 9	−4.82 9	8.84 27(6)
Ma 1	64.43	299.7	0.6222	0.709576 32	0.709311 37	68.79 52	5.616	25.19	0.1348	0.512422 7	−4.22 14	−3.98 14	7.70 27(3)
Mer 1	67.44	353.0	0.5528	0.710190 44	0.709954 47	77.93 66	4.494	20.55	0.1322	0.512368 6	−5.26 12	−5.02 12	8.26 21(3)
Sor 1	65.10	362.8	0.5193	0.710329 52	0.710108 54	80.10 76	6.229	27.83	0.1353	0.512364 4	−5.34 7	−5.11 7	7.70 18(4)
Iorio 2	45.46	290.8	0.4523	0.707384 46	0.707191 48	38.70 68	4.073	18.41	0.1338	0.512504 10	−2.61 19	−2.37 19	7.53 13(4)
Ge 20	64.49	240.9	0.7747	0.708636 34	0.708308 41	54.53 58	3.945	16.83	0.1417	0.512489 22	−2.90 41	−2.70 41	7.53 40(4)
Granodiorite													
Bona 1	199.5	346.4	1.667	0.711078 76	0.710368 90	83.8 1.3	4.624	23.97	0.1166	0.512300 4	−6.60 8	−6.29 8	9.08 32(4)
Shoshonitic Lamprophyre													
P861	251.3	626.2	1.161	0.707779 32	0.707284 46	40.02 65	8.690	50.89	0.1032	0.512425 5	−4.16 10	−3.80 10	7.52 30(7)
Melirolo Augengneis													
Iorio 1	98.41	250.6	1.131	0.715079 25	0.714597 41	143.83 57	5.407	25.91	0.1262	0.512313 5	−6.35 10	−6.07 10	8.67 16(4)
Aplite													
Bona 2	250.0	86.44	8.373	0.715438 46	0.71187 24	105.1 3.4	1.993	8.874	0.1357	0.512263 13	−7.32 26	−7.08 26	9.39 64(5)
Pegmatite													
Siss 7	178.1	48.38	10.67	0.720558 75	0.71601 31	163.9 4.4	1.848	6.383	0.1750	0.512247 11	−7.63 21	−7.54 21	9.86 19(4)
Suretta Roof Pendant													
Bona 3	104.1	219.4	1.374	0.714450 61	0.713865 72	133.4 1.0	5.297	31.63	0.1012	0.512268 14	−7.21 28	−6.85 28	9.81 35(7)

gabbros and discriminated geochemically the MORB type amphibolitic country rocks from the calc-alaline intrusive rocks, and Reusser (1987) by phase petrological and thermal considerations.

One of the major goals of this study is to obtain quantitative data for the origin of the diverse rock types in order to constrain further the possibilities for the genesis of this intrusive complex.

Results

Major and trace element data of the investigated samples are given in Table 1. Isotopic results are given in Table 2. Data for the Novate leucogranite are compiled from the literature: major and trace elements are given by Reusser (1987), REE by Mottana et al. (1978), oxygen isotopes by Diethelm (1989, $\delta^{18}O_{SMOW}=9.10$), and Nd and Sr isotopes by Kagami et al. (1985, $\varepsilon_{Nd}(t)=-8.57$, $^{87}Sr/^{86}Sr=0.709812$). Further data in Figs. 2a and 2b are from Nievergelt and Dietrich (1977), Gautschi and Montrasio (1978), Reusser (1987) and Diethelm (1989).

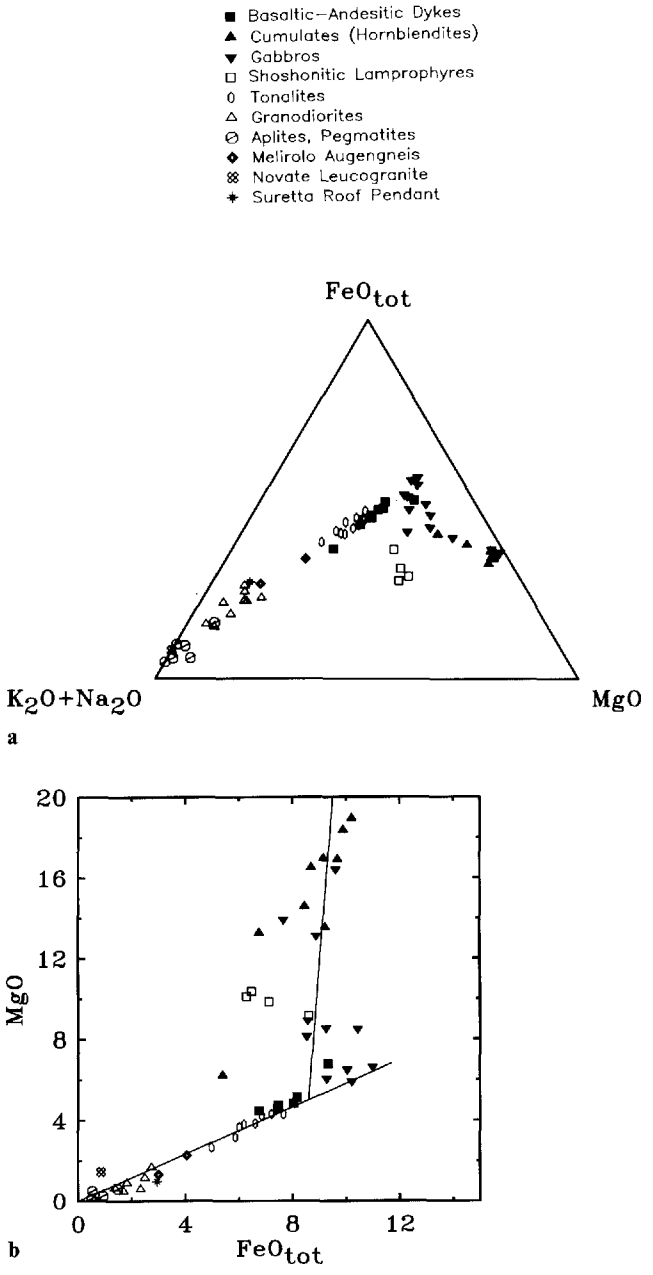

Fig. 2. a AFM-diagram for Bergell samples. Published samples are from Nievergelt and Dietrich (1977), Gautschi and Montrasio (1978), Reusser (1987), and Diethelm (1989). Metasomatically altered basic samples have been avoided. **b** Plot of MgO versusFeO_{tot}. Sample sources- and symbols as in **a**

Major elements

In general, major element geochemistry of the Bergell intrusive rocks defines a clear calc-alkaline trend as shown in the AFM-diagram (Fig. 2a). Two exceptions are recognized: the shoshonitic lamprophyre dykes have an alkaline affinity defined by depletion in total iron relative to the other mafic members (Diethelm 1989); whereas a few gabbros are slightly enriched in total iron.

Fig. 2b shows a plot of MgO versus FeO_{tot} for the same samples as in Fig. 2a. Two distinct trends are visible: a steep decline of MgO at more or less constant FeO_{tot} is displayed by the cumulates and gabbros. This trend can be accounted for by precipitation and removal of olivine and orthopyroxene. The second trend defined by the other members of the suite shows declining MgO and FeO_{tot} and is considered to have been produced by differentiation and/or contamination as will be shown by the isotopic data presented below. As seen in Fig. 2a the basaltic-andesitic dykes have intermediate compositions and plot at the intersection of the two trends. This may well indicate that these dykes were produced by the removal of cumulates but little plagioclase, which would also account for the high aluminium contents of the basalts and andesites. As in Fig. 2a, some gabbros are enriched in total iron, which may be the result of

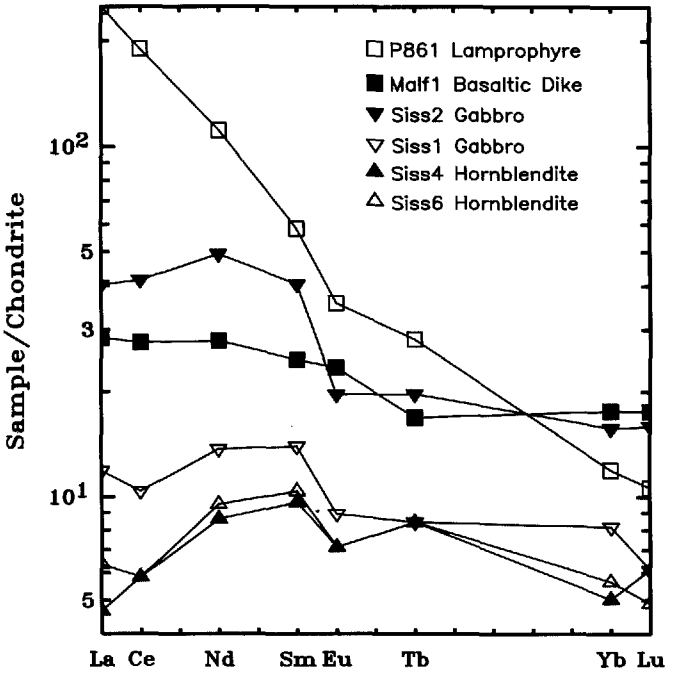

Fig. 3. Chondrite-normalized REE-patterns for basic samples

incomplete differentiation and suppressed fractionation of magnetite. A detailed analysis of the major- and trace-elemental trends of the whole intrusion is given by Reusser (1987). They resemble in most aspects those derived for the very similar south Adamello intrusion (Ulmer et al. 1983).

Rare earth elements

Chondrite-normalized REE patterns of all mafic samples are given in Fig. 3. All cumulates and gabbros plot below the basaltic dyke Malf 1, with the exception of the in situ crystallized gabbro Siss 2. This gabbro appears to have intruded and assimilated country rocks, which is consistent with the strong REE-enrichment and isotopes. The slightly hump-shaped spectra of the cumulitic hornblendites Siss 4 and Siss 6 and the hornblende gabbro Siss 1 are an effect of the dominating hornblende and clinopyroxene.

Table 3. Modes of modelled cumulates (Vol.%) used in calculation of parental melt

	Ol	Opx	Cpx	Hbl	Plag
Siss 1	1		55	38	6
Siss 6	32	5	36	23	4
GS83-2	10		25	50	15
VS86-5d	33		31	34	2
VS86-8	4		40	37	19
Average	16	1	39	34	10

The REE characteristics of the parental melt coexisting with the cumulates are calculated from the concentrations of the cumulates in Table 1, the modes in Table 3, and the partition coefficients of Henderson (1982) and presented in Fig. 4. In addition to the hornblendite Siss 6 and the gabbro Siss 1, the cumulates GS83-2, VS86-8, and VS86-5d of Diethelm (1989) have been added to constrain the melt better. The resulting rare earth patterns (Fig. 4) are rather flat (Ce/Yb = 8.2–14), show small Eu-anomalies, and are 7 to 30 times chondrite. For reference a picrobasalt is also shown. This sample represents the parental magma of the similar Adamello gabbros (Ulmer et al. 1983; Ulmer 1988 and pers. comm.) The calculated parental magmas are similar to the primitive picrobasalt but are lower than the slightly evolved basaltic-andesitic dykes (e.g. Malf 1). It seems most probable that the cumulates were derived from a picrobasaltic magma, and that such a weakly differentiated magma produced the basaltic-andesitic dykes.

REE patterns and isotopic ratios of the tonalites are shown in Fig. 5. La concentrations vary from 120 to 50 times chondrite, Lu from 18 to 9 times chondrite. Ce/Yb varies from 21 (Siss 3, the eastern-most sample) to 11.5 (Ge 20, the western-most sample). Such a LREE enrichment could be produced by hornblende fractionation (Arth and Barker 1976). However, the increase in LREE enrichment is also paralleled by an increase in crustal isotopic ratios, with the exception of the sample Mer 1. Contamination by strongly LREE enriched material in addition to hornblende fractionation may well be the cause for the varying tonalite patterns.

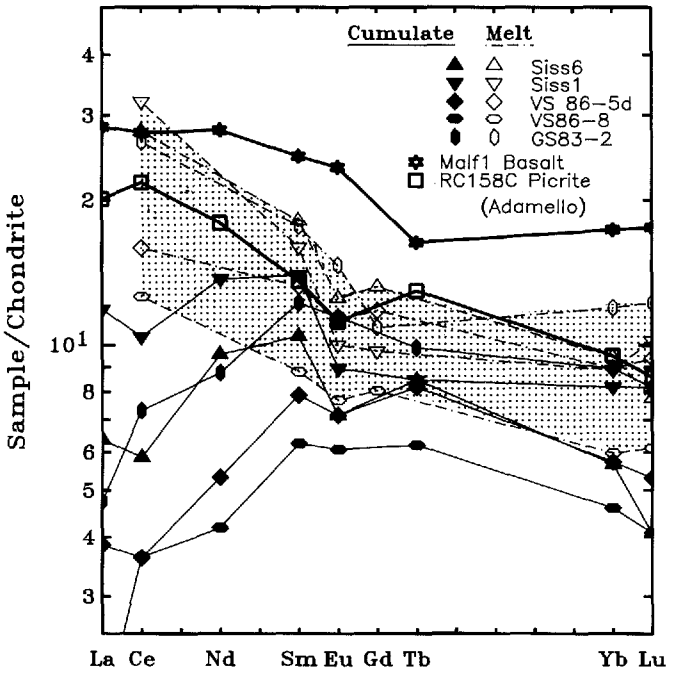

Fig. 4. Chondrite-normalized REE-patterns for cumulates and derived melts. The melts were calculated using the mineral modes given in Table 3 and the partition coefficients for Ce, Sm, Eu, Gd, Yb, and Lu from Henderson (1982). Gd, which was not measured, has been obtained by interpolation between Sm and Tb. The *shaded area* gives the range for primary melts. For comparison, an Adamello picrite-basalt (Ulmer 1988 and pers.comm.) and the Bergell basalt Malf 1 are shown

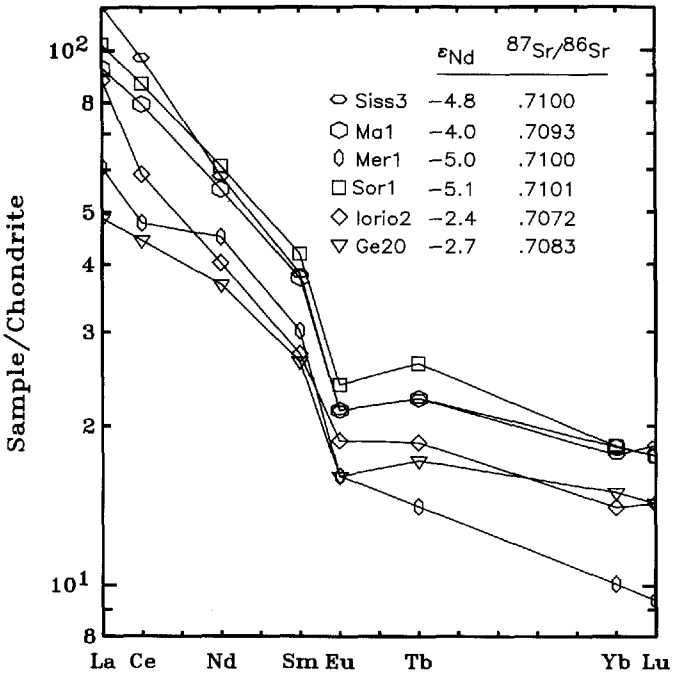

Fig. 5. Chondrite-normalized REE-patterns and isotopic ratios for tonalites

REE patterns of acidic members are plotted in Fig. 6. As an example for a potential crustal contaminant, the roof pendant, Bona 3, is also displayed and shows the steepest rare earth pattern with the highest LREE/HREE enrichment. The granodiorite, Bona 1, which plots intermediately between the tonalites (shaded area) and the roof pendant, could be produced by AFC contamination of a tonalite with a material such as that represented by the roof pendant. Hornblende fractionation as sole process (Arth and Barker 1976) is excluded by the isotopic data (see below). The same argument also holds for the Melirolo Augengneis, Iorio 1. Aplite, pegmatite, and the Novate leucogranite are all strongly depleted and show very large Eu anomalies. This may imply that REE and Eu bearing minerals (accessories, feldspar) have been fractionated before the formation of these rocks or that the fused country rock retained the accessories in the residue.

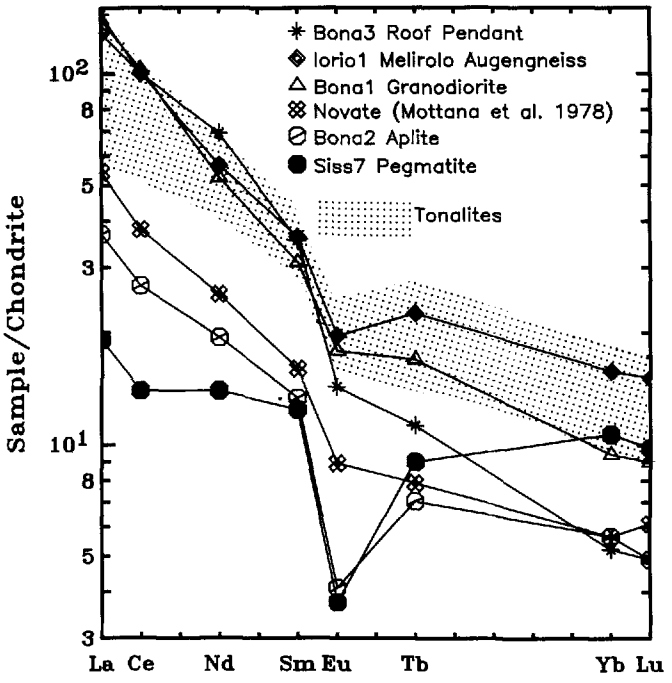

Fig. 6. Chondrite-normalized REE-patterns for acidic samples and range (*shaded*) for tonalites

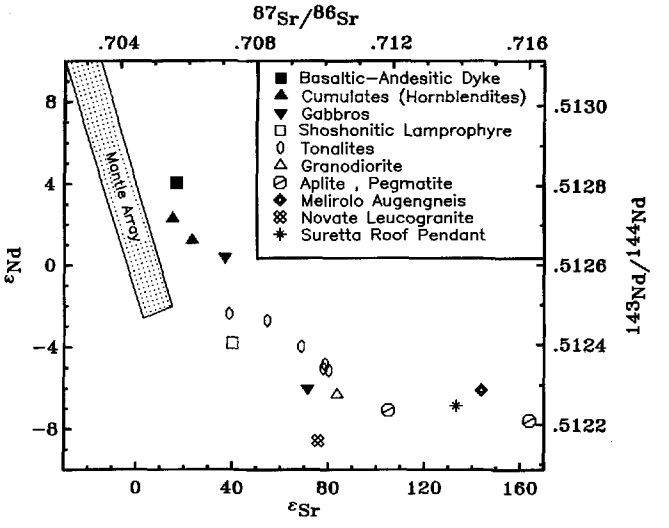

Fig. 7. ε_{Nd} versus ε_{Sr} diagram time corrected to 30 Ma. The "mantle array" is after DePaolo (1988). The Novate data point is from Kagami et al. (1985)

Isotopic results

All the results obtained by isotope dilution and isotopic ratios are given in Table 2.

The Sr- and Nd-isotope data, corrected for 30 Ma, are shown in Fig. 7 and compared with other circum-Mediterranean Tertiary plutons in Fig. 8. There are several features of note: (a) the array starts at ε_{Nd} of +4.0 for the mantle endmember as does the Adamello array (Kagami et al. 1991). (b) Compared with the mantle array and the Adamello field, all Bergell $^{87}Sr/^{86}Sr$-ratios are elevated for a similar ε_{Nd}-value, whereby no real $^{87}Sr/^{86}Sr$ mantle-value is observed. (c) The Novate leucogranite is displaced away from the array towards lower ε_{Nd} (−8.6) and lower $^{87}Sr/^{86}Sr$ (0.7098). These data are consistent with bulk-rock geochemical data (Gulson 1973; Reusser 1987) which indicate that the Novate leu-

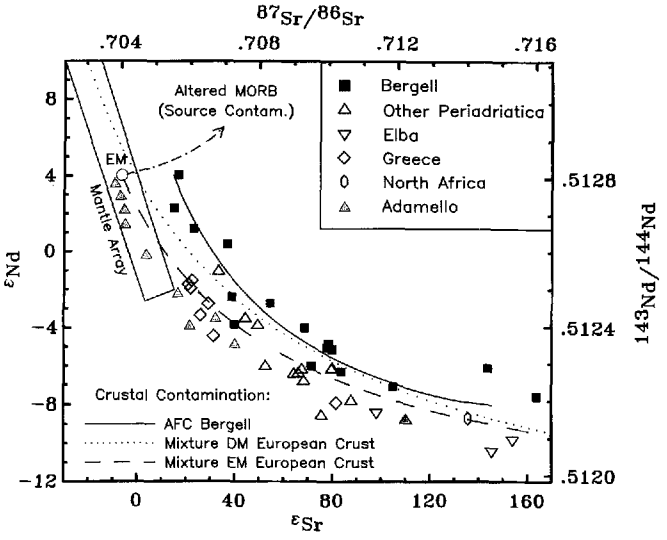

Fig. 8. Same diagram as Fig. 7 but with comparison of the Bergell (*solid symbols*) with other Mediterranean plutonic rocks (*open symbols*). The Adamello data are from Kagami et al. (1991); "Other Periadriatica" from Kagami et al. (1985), Juteau et al. (1986), Barth et al. (1989); Elba, Greece, and North Africa from Juteau et al. (1986). Three crustal contamination curves are shown: The *solid curve* represents an AFC curve (DePaolo 1981, r=0.5, D_{Nd}=0.3, D_{Sr}=0.4) between a picrobasaltic partial melt originating from a contaminated enriched mantle as proposed for the Bergell magma source (ε_{Nd}=+4, $^{87}Sr/^{86}Sr$=0.7055) and European crust. The *dotted curve* represents a hypothetical simple mixture between a picrobasaltic partial melt (Table 4) with isotopic characteristics of depleted mantle (DM) and European crust. The *dashed curve* represents a simple mixture between a picrobasaltic partial melt originating from enriched mantle (EM) and European crust, as invoked for the other Periadriatic intrusions. A source contamination curve (*dashed-dotted*) is given for a simple mixture between enriched mantle and altered MORB. A source contamination curve for pelagic sediments roughly parallels the dashed curve but is omitted for clarity. See Table 4 for properties of endmembers

cogranite is unrelated to the Bergell intrusion and is derived from a different source. (d) Whereas all mafic samples are within the mantle field with respect to ε_{Nd}, the gabbro Siss 2, which intruded country rocks, shows highly crustal ε_{Nd} and $^{87}Sr/^{86}Sr$. (e) The Bergell tonalite is isotopically very heterogenous. The main body (Siss 3, Ma 1, Mer 1, Sor 1) has more crustal values ($\varepsilon_{Nd} = -4$ to -5.1, $^{87}Sr/^{86}Sr = 0.709$ to 0.710) than the Iorio tonalite (Iorio 2, Ge 20: $\varepsilon_{Nd} = -2.4$ to -2.7, $^{87}Sr/^{86}Sr =$ 0.707 to 0.708). (f) The Melirolo Augengneis, Iorio 1, which is closely associated with the Iorio tonalite, Iorio 2, yields much more crustal ε_{Nd} (-6.1 versus -2.4) and $^{87}Sr/^{86}Sr$ (0.715 versus 0.707) which suggests that significant assimilation would have had to take place to generate the Augengneis from the tonalite.

$\delta^{18}O$ versus ε_{Nd} is shown in Fig. 9. The oxygen isotope compositions range from mantle to crustal values. This variation is too high to be produced by mineral fractionation alone which would account for only a 1‰ shift (James 1981). The samples are well correlated. All mafic samples with one exception plot within the mantle field (the field defined by continental tholeiites and alkali basalts with respect to $\delta^{18}O$, Kyser 1990, and the whole mantle with respect to Nd). They are relatively homogeneous in oxygen but vary in Nd. The tonalites and the shoshonitic lamprophyre are intermediate in both Nd and oxygen. All acidic members and the in situ gabbro display strongly crustal Nd as well as oxygen. The trend of the acidic samples is rather smooth because ε_{Nd} for the crustal endmembers is restricted to a limited range.

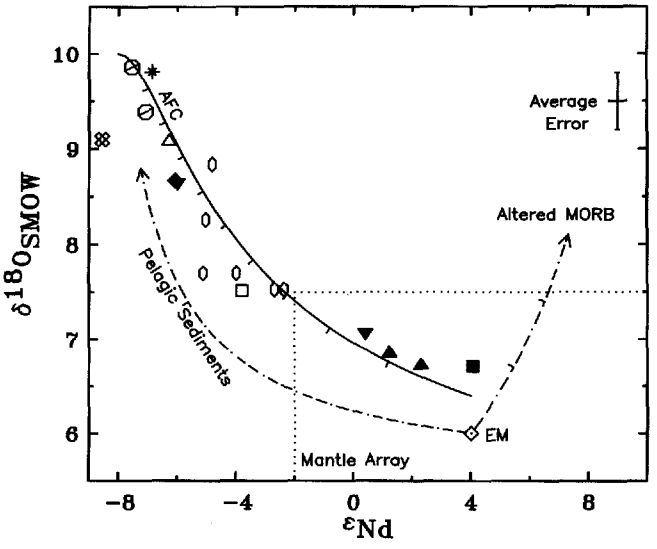

Fig. 9. $\delta^{18}O$ versus ε_{Nd}-plot. The "Mantle Array" is after Kyser (1990, $\delta^{18}O$ assumed for the subcontinental lithospheric mantle from continental tholeiites and alkali basalts) and DePaolo (1988, ε_{Nd} in oceanic basalts, as no precise estimates are available for the range of Nd-compositions in the continental mantle). The Bergell data can be fitted with an AFC curve (parameters as in Fig. 8) between a picrobasaltic partial melt originating in a source-contaminated enriched mantle and European crust. Source contamination curves are shown for enriched mantle contaminated by altered MORB and pelagic sediments. Endmembers are given in Table 4. The *tickmarks* shown are for every 10 weight % contaminant in magma or mantle

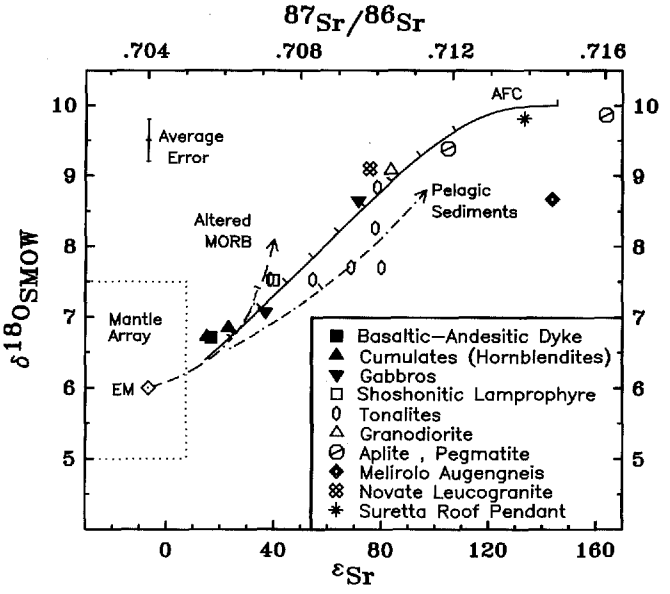

Fig. 10. $\delta^{18}O$ versus ε_{Sr}-plot. The "Mantle Array" field is as in Fig. 9, ε_{Sr} is after DePaolo (1988). Mixing curves correspond to the same processes as in Fig. 9

A noteworthy feature is displayed by the $\delta^{18}O$ versus $^{87}Sr/^{86}Sr$ diagram (Fig. 10): while the mafic samples range within the mantle field with respect to $\delta^{18}O$, all $^{87}Sr/^{86}Sr$ values are crustal. The acidic samples scatter widely in both $^{87}Sr/^{86}Sr$ and $\delta^{18}O$, which is expected in the light of the heterogeneous nature of the potential crustal endmembers.

Discussion

The endmembers

Two endmembers can be distinguished on the basis of whole-rock geochemical data and isotopic compositions. The first endmember is a picrobasaltic partial melt originating in the mantle; the second are crustal rocks. The origin of the mantle endmember can now be assessed.

One source for the Bergell magmas could be the depleted mantle (DM, characteristics given in Table 4). A mixture between a DM partial melt and 'European type' crust is indicated by the dotted curve in Fig. 8. This model applied solely for the Bergell could crudely explain the shift of the basic units towards more radiogenic Sr composition at similar mantle Nd when compared with other circum-Mediterranean intrusions (Fig. 8).

However, considering their very similar geological settings, an origin in enriched mantle (EM) for both Bergell and Adamello seems much more likely. Both Nd and oxygen yield mantle values for the cumulates and the basalt-andesite Malf 1, and the ε_{Nd} of +4 of this latter sample is typical for the Central European subcontinental mantle at this time (Stille 1987; Stille et al. 1989). This is also the highest ε_{Nd} obtained in the neighbouring Adamello batholith (Kagami et al. 1991). According to Wilson and Downes (1991) an ε_{Nd} of +4 would corre-

Table 4. Properties of endmembers taken for isotopic mixing models. The sources are a) Taylor (1980); b) James (1981); c) Faure (1986); d) Stille (1987) and unpublished calculations, also average asthenospheric-lithospheric mantle mix value of Wilson and Downes (1991); e) Ulmer (1988) and pers. comm.; f) Yeh (1980); g) Wedepohl (1978); h) Average European Basement, Liew and Hofmann (1988); i) Elderfield et al. (1981); j) Tethys seawater, Stille and Fischer (1990); k) Quartz Alpine Basement, Hoernes and Friedrichsen (1980); l) Kyser (1990)

Component	$\delta^{18}O$	ppm Sr	$^{87}Sr/^{86}Sr$	ppm Nd	ε_{Nd}
Depleted Mantle	+5.7[a]	not used	0.703[b]	not used	+10[c]
Enriched Mantle	+6.0[l]	46 ppm[d]	0.704[d]	3.5 ppm[d]	+4[d]
Enriched Mantle Picrobasaltic partial melt	+6.0[l]	167 ppm[e]	0.704[d]	8.2 ppm[e]	+4[d]
Pelagic Sediments	+20[f]	200 ppm[g]	0.718[h]	90 ppm[i]	−9[j]
Altered MORB	+13[a]	500 ppm[b,c]	0.708[a,b]	10 ppm[c]	+10[c]
Alpine Crust	+10[k]	100 ppm[h]	0.718[h]	20 ppm[h]	−10[h]

spond to a mixture of asthenospheric and lithospheric sub-European mantle. The enrichment in radiogenic Sr (+0.002) in the Bergell rocks as compared with the Adamello is discussed below.

The other endmember in the main mixing and contamination process is the considerably heterogeneous lower and middle Alpine crust. Present day depth estimates for this crust are up to 60 km (Bernoulli et al. 1990), the depth of the cumulate formation was estimated to be about 30 km (Diethelm 1989), and the level now exposed in the Bergell area was buried at a depth of 20–30 km (Reusser 1987). Thus considerable thickness of crust had to be traversed by the rising magma during which assimilation took place. Average values for the assimilated crust are given in Table 4; note however, that $^{87}Sr/^{86}Sr$ scatters enormously in the exposed Alpine nappes. Further constraints for the Nd-composition of the crustal endmember comes from an ε_{Nd} of −8.1 which was measured on a zircon fraction from the granodiorite, which can be attributed to the inheritance of old cores, with a much lower ε_{Nd} than the bulk rock value of −6.3 (von Blanckenburg 1990). The roof pendant Bona 3 and the pegmatite Siss 7 are therefore close to the isotopic composition of the expected average endmember.

The shift of $^{87}Sr/^{86}Sr$ in the mafic endmembers

A characteristic feature of the Bergell trend is the displacement of the basic units away from the mantle array towards more radiogenic Sr. This shift is correlated with a slight increase in $\delta^{18}O$ from a "real" mantle value of ~+6‰ to values of ≥6.7‰. Such a displacement can be generated by three possible processes:

(A) Subsolidus alteration. This may effect not only the whole-rock oxygen values in basalts (Kyser 1990), but also the margins of intrusions affected by circulating hydrothermal fluids. At the high temperatures of the intrusion, with an origin in metapelitic or calcareous country rock, such hydrothermal fluids could potentially produce a strong elevation in $\delta^{18}O$ and possibly a slight increase of $^{87}Sr/^{86}Sr$ ratio in the solidified intrusive rocks (Hill et al. 1986). At the present stage it is difficult to assess rigorously whether such a process may have acted by the younger tonalite melt enclosing the already solidified gabbroic and cumulitic bodies. However, several arguments suggest that the isotopic signatures are of primary origin: (1) Most of the samples display a primary igneous mineral assemblage without indications of recrystallization. (2) Only large mafic bodies devoid of enrichments in alkalies were investigated. The small bodies enriched in alkali elements at the western margin of the intrusion (Diethelm 1989, p. 54) have been carefully avoided. (3) The early basaltic dyke, Malf 1, displays the same elevated $\delta^{18}O$ and $^{87}Sr/^{86}Sr$ characteristics, although it intruded far outside of the later contact aureole of the intrusion and in a greenschist metamorphic environment consisting of ophiolitic serpentinite. Exchange with crustal Sr or oxygen must be excluded for this sample. (4) The predominant exchange mechanism for Sr and O in the cumulitic bodies would be diffusion, as the permeability at the high temperatures of the later tonalite intrusion would be low (Dickin et al. 1980). It is likely, however, that the bodies, which are ≥100 m in diameter, would have been too large to be infiltrated as a whole by diffusive transport. Thus, it is concluded that at least the observed Sr-isotopic features are of primary origin.

(B) Lower crustal amphibolite melting. In continental collision zones undergoing extension, amphibolites may melt in the lower crust without heat transfer from mantle-derived melts (England and Thompson 1986). The partial melts formed would be granitic to tonalitic. Underplating of the lower crust by basaltic partial mantle melts could lead to andesitic or even high-alumina basaltic melts. Such a process operating in the Ivrea zone (Southern Alps) was suggested to have generated the South-Alpine Hercynian granites and andesites (Stille and Buletti 1987). The corresponding lower crustal magma chamber processes have been studied by Voshage et al. (1990) in the Ivrea zone. Since the mafic lower

crust is in general enriched in $\delta^{18}O$ (average $\delta^{18}O = 7.5‰$, Fowler and Harmon 1990) an origin of the Bergell melts in the lower crust could explain their elevated $\delta^{18}O$ values. However, as in the neighbouring Adamello intrusion (Ulmer et al. 1983; Kagami et al. 1991), the presence of isotopically primitive cumulates and gabbros, for which REE modelling indicates a picrobasaltic and thus mantle-derived parental melt (Fig. 4), provides strong evidence that the intrusion originated in the mantle and contains a significant primary mantle component. Moreover, crustal melting alone would result in a clustering of data, whereas the smooth isotopic mantle-crust mixing trends, which correlate well with degree of differentiation, strongly suggest that AFC mixing between mantle and crustal endmembers was the governing process. In summary the large volumes of tonalite present (Fig. 1) indicate that the amphibolitic lower crust may have been the predominant location for assimilation and generation of the *tonalitic magmas* but the elevations in $^{87}Sr/^{86}Sr$ and $\delta^{18}O$ of the *basic early differentiates* are a primary feature inherent to the partial mantle melt.

(C) Mantle source contamination. Source contamination models are generally invoked for the genesis of island arc basalts (e.g., Davidson and Harmon 1989; Chen et al. 1990, for two recent examples and references therein), but have also been taken to account for continental volcanic arcs (Stern et al. 1990). The shift to the right in the ε_{Nd} versus ε_{Sr} diagram and the elevation of the $\delta^{18}O$ can be explained by subducted and seawater-altered MORB basalts (Hawkesworth et al. 1977) contaminating the mantle source of the Bergell magma by fluid release or partial melting. Given the properties of enriched mantle, EM, ($^{87}Sr/^{86}Sr = 0.704$, $\delta^{18}O = 6.0$), and altered MORB ($^{87}Sr/^{86}Sr = 0.708$, $\delta^{18}O \leq +13‰$),the resulting mixing curves between these two components are shown in Figs. 8, 9, and 10 (see Table 4 for references). An alternative potential mantle contaminant would be carbonate rocks, as these too contain high Sr but are very low in Nd.

The isotopic evolution is best explained by the ε_{Nd} versus $\delta^{18}O$ diagram (Fig. 9). The enriched mantle is firstly contaminated by altered MORB which results in a strong elevation in $\delta^{18}O$ and a slight elevation in ε_{Nd}. The latter offset can be compensated simultaneously or successively by additional input of subducted sediment or even continental crust, which would shift the EM composition into the direction indicated by the pelagic sediment curve. The resulting mixture of EM, altered MORB, and sediments defines the starting point for the generation of picrobasaltic magma.

From this point on, the process of crustal contamination by continental crust would be operative. The evolution of ε_{Nd}, $^{87}Sr/^{86}Sr$, and $\delta^{18}O$ is best approximated with a reference AFC curve (DePaolo 1981, solid curves in Figs. 8, 9, 10 and the parameters given in the caption of Fig. 8).

The Bergell data set is thus consistent with a two stage contamination model: primary contamination of an enriched mantle source by dehydration and fluid release or partial melting of strongly altered MORB and little sediment or continental crust, then contamination of partial melts generated in this mantle by continental Alpine crust, with simultaneous fractional crystallization. A similar interference of source and crustal contamination processes was proposed for an island arc by Davidson and Harmon (1989).

The role of the shoshonitic lamprophyre

The shoshonitic lamprophyre P861, which is a "minette" in mineralogical terms, can be explained by originating directly in a deep-seated mantle magma source and being emplaced with little or no differentiation. Accordingly for the steep REE pattern and strong LREE enrichment (Fig. 3), Diethelm (1989) calculated a 3% partial melting of a 4–7 times LREE-enriched garnet-lherzolitic mantle as the source for such a melt. This is consistent with isotopic models (Turpin et al. 1988; Stille et al. 1989), which suggest melting of a mantle enriched by sedimentary melts as a source for minettes. That these source contamination models are also valid for the Bergell lamprophyre P861 is indicated by ε_{Hf} corrected to 30 Ma of -2.2 ± 1.6 for a zircon and -1.2 ± 2.9 for the whole-rock of this sample (Stille and Steiger 1991). This compares with an ε_{Nd} of -3.8 (Table 2) and supports the involvement of sediment subducted into the mantle source.

Deep lithospheric structure and magma emplacement

The displacement of the Bergell array towards more radiogenic $^{87}Sr/^{86}Sr$ by source contamination may well be a unique feature of this intrusion in comparison with all other circum-Mediterranean plutons (Fig. 8). However, a simple Andean-type subduction model may not account for the complex geodynamic situation in the Alps: evidence for subduction of *continental* crust is given by exposed high-pressure rocks in the Western Alps (Tilton et al. 1989). Seismic profiles (Bernoulli et al. 1990) suggest that European continental crust (and Tethyan oceanic crust) was subducted below the Adriatic moho. On the other hand, a slab of Adriatic lower crust was emplaced below the Central Alpine area at a present day depth of ~ 30 km (Bernoulli et al. 1990, Fig. 6). Assuming a magma generation depth of ~ 60 km, which would be the present day depth of the European moho below the Bergell area, it is quite possible that the generation of Bergell magma predates the underplating by the Adriatic lower crust, as the latter could have prevented the ascent of magma.

The evolution following the source contamination may be approximated in the following manner. The picrobasaltic mantle melts fed a magma chamber, evidence for which is given by the presence of cumulates and the fact that tonalites are not produced directly in the mantle source (Wyllie et al. 1976). The depth of the magma chamber can be estimated to be at ~ 30 km (Diethelm 1989). Differentiation of these melts in the magma

chamber led to accumulation of hornblendites and pyroxenites and to the evolution of the basaltic-andesitic melts, which first intruded into the country rocks. Then assimilation started with simultaneous fractional crystallization and produced the tonalites. Different magma batches exhibiting varying degrees of contamination rose from the magma chamber and equilibrated at continuously decreasing depth. This accounts for both the lower crustal contamination, and the lesser enrichment in LREE in the deeper, western tonalite than in the shallower central and eastern tonalite. During ascent the tonalitic magmas dragged solidified megablocks of cumulates with them from the magma chamber. Local differentiation during the tonalite emplacement produced in situ formation of the highly crustal gabbros. Further AFC processes led to the generation of the granodiorite and perhaps the Melirolo Augengneis. The zoned structure of the Bergell batholith (Fig. 1) provides some evidence that the emplacement of the granodiorite intrusion involved some kind of ballooning process (Halliday 1983): the primary magma (tonalite) intruded country rocks and solidified from the margins inward. Later the granodiorite melt rose through the central core of tonalite, which was not solidified by crystallization – in contrast to the cooling margins – and "ballooned out" the top of the intrusion. Simultaneously, shoshonitic lamprophyres intruded with little modification from the mantle source. As a final stage, the pegmatites and aplites were produced from residual liquids and, locally, fused country rock during the final emplacement of the intrusion.

Conclusions

A combination of both radiogenic- and stable-isotope methods allows the identification of several components contributing to the genesis of the Bergell igneous complex. In a first stage, the mantle source, which has been identified as an enriched subcontinental mantle, is contaminated by a material containing radiogenic Sr and high $\delta^{18}O$. Strongly seawater-altered oceanic crust or carbonates are considered to have been subducted and to have released fluids into this mantle. A small amount of continental material, such as sediments or crust, may have also contributed to the source contamination process. This source contamination process may have predated the generation of partial mantle melts inducing the intrusion.

In a second stage, which takes place in the thickened Alpine crust, partial melts from the contaminated mantle segment introduce cumulate formation, dyke intrusion, and crustal melting which produce the acidic members of the intrusion by AFC processes. An origin of the whole suite by lower crustal amphibolite melting is considered unlikely due to the presence of ultramafic cumulates, but such a process may have contributed to the large volumes of tonalite.

If the described features are indeed due to source contamination processes, which are known to contribute to the genesis of island- or continental volcanic arcs, it must be concluded that these may also be of importance in calc-alkaline pluton genesis. In the case of the Tertiary Alpine intrusions, source contamination so far appears to have operated in the case of the Bergell intrusion only.

Acknowledgements. The isotope part of this research project was proposed by R.H. Steiger, who also commented on an earlier version of this manuscript. F. Oberli provided data aquisition and reduction programmes as well as many helpful discussions. M. Meier maintained the chemistry lab. V. Trommsdorff provided sample Malf 1. V. Trommsdorf, M. Bickle and K. Burton made helpful comments on this manuscript. The sample Ge 20 was provided by E. Reusser. H.R. Fisch and E. Reusser participated in field trips. U. Mok and M. Tuchschmid performed the INA analyses. P. Ulmer supplied unpublished data. D. Blamart (TU München) kindly remeasured the oxygen isotopes. The reviews by R. Harmon and W. Frank are gratefully acknowledged. To all these individuals we express our sincere thank. This work has been supported by ETH grant No. 0.330.085.51/5 and Schweiz. Nationalfonds grant No. 20-5095.86.

Appendix 1

Analytical methods

Bulk chemical compositions were determined by XRF analysis at the Eidgenössische Materialprüfungsanstalt in Dübendorf (Switzerland) following the procedure given in detail by Reusser (1987). The relative error for major elements is 2% in the 4–100% concentration range, about 10% for smaller concentrations. FeO was determined by $KMnO_4$ titration; H_2O by loss on ignition. The relative analytical errors for trace elements are 2–10% for the 10–100 ppm concentration range, the accuracy is 5% for the 1000 ppm-, ~10% for the 100 ppm-, and ~20% for the 10 ppm-range.

REE and U, Th, and Hf concentrations were measured by instrumental neutron activation analysis at the Paul Scherrer Institut in Würenlingen (Switzerland). Count statistical errors are ≤10%. Comparison with isotope dilution data for Sm and Nd yields reproducibilities within this range.

Oxygen isotope analyses were carried out at the new facilities of the Institut für Mineralogie und Petrographie, ETH Zürich. All powders were rinsed in cold HCl to remove possible traces of carbonates. Oxygen was liberated by reaction with ClF_3 at 600° C and converted to CO_2. $^{18}O/^{16}O$ ratios were measured on a VG micromass 903 mass spectrometer and reported relative to SMOW. Measurements of NBS-28 yielded $\delta^{18}O_{SMOW} = 9.58 \pm 0.26$ (SD) during the course of this work. All samples were analyzed in replicate, and control measurements were additionally performed at the Institut für angewandte Mineralogie und Geochemie, TU München, Fed. Rep. of Germany; the results are used for mean values in Table 2. For all sets of replicate oxygen measurements, one standard deviation is given.

Rb, Sr, Sm and Nd concentrations were measured by isotope dilution using mixed ^{85}Rb-^{84}Sr and ^{149}Sm-^{150}Nd spikes. 100–150 mg of rock powder was spiked and dissolved using the bomb technique of Krogh (1973). Rb, Sr and REE were separated by cation exchange resin eluting with 2.5 and 6 M HCl, respectively. Sm and Nd were then separated by cation exchange resin with alpha-hydroxy-isobutyric acid. Blanks were approximately 1 ng for Sr, 11 ng for Rb, 0.18 ng for Nd, and 0.02 ng for Sm. These blanks were negligible, compared with the sample contents.

Concentration and isotopic composition were measured together. Sr was measured on a Tandem Varian MAT mass spectrometer. During the course of this study, 5 runs of SRM 987 yielded an average $^{87}Sr/^{86}Sr$ of 0.710260 ± 77 (2 sigma standard deviation),

two runs of BCR-1 yielded 0.705003±38 and 0.705023±42. Rb, Sm, and Nd were measured on a Finnigan MAT261 mass spectrometer. Standard runs of Rb yielded a 2 sigma deviation of 0.6% for mass fractionation. Three Nd isotopes were measured simultaneously on a static multicollector. In addition to the electronic gain calibration, $^{143}Nd/^{144}Nd$ ratios were corrected for small inter-collector bias by using the $^{145}Nd/^{146}Nd$ ratio, which was measured on the same collectors. Ratios were normalized to $^{146}Nd/^{144}Nd = 0.7219$. Using these corrections, 20 runs of Nd-β (Wasserburg et al. 1981, $^{143}Nd/^{144}Nd = 0.511928$) yielded a $^{143}Nd/^{144}Nd$ of 0.511916±16 (2 sigma standard deviation). Three runs of BCR-1 yielded $^{143}Nd/^{144}Nd$ of 0.512643±22, 0.512647±17, and 0.512647±10 (95% C.L. error of the mean).

Time corrections were calculated using decay constants of $1.42*10^{-11}$/year for ^{87}Rb and $6.54*10^{-12}$/year for ^{147}Sm (DePaolo 1988). An error of 0.6% for $^{87}Rb/^{86}Sr$ and t=±2 Ma was propagated into time-corrected $^{87}Sr/^{86}Sr$ ratios. The effect of this correction on $^{143}Nd/^{144}Nd$ errors was negligible. ε_{Sr} and ε_{Nd} were calculated using $^{87}Sr/^{86}Sr_{UR} = 0.7045$; $^{87}Rb/^{86}Sr_{UR} = 0.0827$; $^{143}Nd/^{144}Nd_{CHUR} = 0.512638$, and $^{147}Sm/^{144}Nd = 0.1967$.

Appendix 2

Sample locations and mineralogy

Explanation: Sample No.; Non-rigorous petrographic description; Swiss grid coordinates; altitude; location; major mineralogy

Abbreviations: Cpx = Clinopyroxene, Opx = Orthopyroxene, Ol = Olivine, Plag = Plagioclase, Hbl = Hornblende, Bio = Biotite, Musc = Muscorite, Qz = Quartz, Kfs = Kfeldspar, Epi = Epidote, Zoi = Zoisite, Opq = Opaques

BONA 1: Granodiorite; 776.80/132.40; 2550 m; Val Bona, Ridge below Cima di Val Bona; Plag > Kfs > Qz > Bio > Hbl

BONA 2: Aplite; 775.90/133.50; 2820 m; Val Bona, at Sella del Forno; Qz > Kfs > Plag

BONA 3: Suretta Roof-Pendant (Bio-Gneiss); 775.75/132.95; 2820 m; Val Bona, Ridge below Monte Rosso, Boulder; Plag > Kfs > Qz > Bio

GE 20: Tonalite; 730.50/115.70; 1890 m; Iorio Pass, Alpe Gesero; Plag > Hbl > Bio > Qz > Epi

IORIO 1: Melirolo Augengneiss (Granodiorite with Plag-Augen); 732.88/144.60; 2190 m; Iorio-Pass, Cima di Cugn; Plag > Qz > Bio > Epi

IORIO 2: Tonalite; 734.12/115.40; 1850 m; Iorio-Pass, at Alpe la Boga; Plag > Hbl > Bio > Qz > Epi

MA 1: Tonalite; 769.05/119.60; 900 m; Valle Masino, Quarry SW Categgio; Plag > Hbl > Bio > Qz > Epi

MALF 1: Basaltic Dyke; 784.25/128.15; 1980 m; Between M. Braccia and Chiesa, in Malenco serpentinite; Plag > Hbl > Zoi

MER 1: Tonalite; 754.30/115.70; 200 m; Valle Mera, Quarry N Nuova Olonia; Plag > Hbl > Bio > Qz > Epi

P861: Shoshonitic Lamprophyre; 767.45/126.90; 2560 m; Valle Porcelizzo, SW Punto Camerozzo; Hbl > Kfs > Plag > Cpx > Bio

SISS 1: Hornblende-Gabbro; 777.30/130.20; 2460 m; Valle Sissone, Vazzeda Ridge; Cpx > Hbl > Plag > Ol

SISS 2: In-situ crystallized gabbro; 776.35/130.35; 2760 m; Valle Sissone, Vazzeda Ridge; Hbl > Plag > Bio > Sphene

SISS 3: Tonalite; 777.10/129.90; 2450 m; Valle Sissone, below Sissone-Glacier; Plag > Hbl > Bio > Kfs > Epi

SISS 4: Hornblendite; 778.05/130.10; 1990 m; Valle Sissone, Valley-path near creek; Hbl > Cpx > Plag > Talc > Opq

SISS 6: Pyroxenite; 777.30/130.45; 2400 m; Valle Sissone, Alpe Sissone, Boulder; Cpx > Ol > Hbl > Opx > Plag

SISS 7: Pegmatite; 777.35/131.50; 2480 m; Valle Sissone, N Rifugio Del Grande; Plag > Qz > Kfs > Musc > Bio

SOR 1: Tonalite; 749.30/115.39; 210 m; Sorico, new road outcrop; Plag > Hbl > Epi > Bio > Qz

References

Arth JG, Barker F (1976) Rare-earth partitioning between hornblende and dacitic liquid and implications for the genesis of trondhjemitic-tonalitic magmas. Geology 4:534–536

Barth S, Oberli F, Meier M (1989) U–Th–Pb systematics of morphologically characterized zircon and allanite: a high-resolution isotopic study of the Alpine Rensen pluton (northern Italy). Earth Planet Sci Lett 95:235–254

Bernoulli D, Heitzmann P, Zingg A (1990) Central and southern Alps in southern Switzerland: tectonic evolution and first results of reflection seismics. In: Roure F, Heitzmann P, Polino R (eds) Deep structure of the Alps. Mém Soc géol France 156; Mém Soc géol suisse 1; Geol Soc Ital, Vol spec 1:289–302

von Blanckenburg F (1990) Isotope geochemical and geochronological case studies of Alpine magmatism and metamorphism: the Bergell intrusion and Tauern Window. PhD dissertation ETH Zürich

Chen C-H, Shieh Y-N, Lee T, Chen C-H, Mertzman SA (1990) Nd–Sr–O isotopic evidence for source contamination and an unusual mantle component under Luzon Arc. Geochim Cosmochim Acta 54:2473–2483

Clondiffe E, Mottana A (1974) Studio sperimentale del «serizzo» a moderate pressioni. Soc It Mineral e Petrol 30:919–930

Davidson JP, Harmon RS (1989) Oxygen isotope constraints on the petrogenesis of volcanic arc magmas from Martinique, Lesser Antilles. Earth Planet Sci Lett 95:255–270

DePaolo DJ (1981) Trace element and isotopic effects of combined wallrock assimilation and fractional crystallization. Earth Planet Sci Letters 53:189–202

DePaolo DJ (1988) Neodymium isotope geochemistry. Springer, Berlin Heidelberg New York

Dickin AP, Exley RA, Smith BM (1980) Isotopic measurement of Sr and O exchange between meteoric-hydrothermal fluid and the Coire Uaigneich granophyre, Isle of Skye, N.W. Scotland. Earth Planet Sci Lett 51:58–70

Diethelm K (1985) Hornblendite und Gabbros im östlichen Bergell (Val Sissone, Provinz Sondrio, Italien). Schweiz Mineral Petrogr Mitt 65:223–246

Diethelm K (1989) Petrographische und geochemische Untersuchungen an basischen Gesteinen der Bergeller Intrusion. PhD dissertation ETH-Zürich

Drescher-Kaden FK (1940) Beiträge zur Kenntnis der Migmatit- und Assimilationsbildungen, sowie der synantetischen Reaktionsformen. I. Über Schollenassimilation und Kristallisationsverlauf im Bergeller Granit. Chem Erde 12:157–238

Elderfield H, Hawkesworth CJ, Greaves MJ, Calvert SE (1981) Rare earth element geochemistry of oceanic ferromanganese nodules and associated sediments. Geochim Cosmochim Acta 45:513–528

England PC, Thompson AB (1986) Some thermal and tectonic models for crustal melting in continental collision zones. In: Coward MP, Ries AC (eds) Collision tectonics. Geol Soc London Spec Pub 19:83–94

Faure G (1986) Principles of isotope geology, 2nd edn. John Wiley & Sons, New York

Fowler MB, Harmon RS (1990) The oxygen isotope composition of lower crustal granulite xenoliths. In: Vielzeuf D, Vidal P (eds) Granulites and crustal evolution. Kluwer Academic Publishers, Dordrecht, pp 493–506

Gautschi A, Montrasio A (1978) Die andesitisch-basaltischen Gänge des Bergeller Ostrandes und ihre Beziehung zur Regional- und Kontaktmetamorphose. Schweiz Mineral Petrogr Mitt 58:329–343

Gulson BL (1973) Age relations in the Bergell region of the south-east Swiss Alps: with some geochemical comparisons. Eclogae Geol Helv 66:293–313

Gulson BL, Krogh TE (1973) Old lead components in the young Bergell massif, south-east Swiss Alps. Contrib Mineral Petrol 40:239–252

Halliday AN (1983) Crustal melting and the genesis of isotopically and chemically zoned plutons in the Southern Uplands of Scotland. In: Atherton MP, Gribble CD (eds) Migmatites, melting and metamorphism. Shiva publ ltd, Nautwich, pp 54–61

Hawkesworth CJ, O'Nions RK, Pankhurst PJ, Hamilton PJ, Evenson NM (1977) A geochemical study of island-arc and back-arc tholeiites from the Scotia Sea. Earth Planet Sci Lett 36:253–262

Henderson P (1982) Inorganic geochemistry. Pergamon, Oxford

Hill RI, Silver LT, Taylor HP (1986) Coupled Sr–O isotope variations as indicator of source heterogeneity for the Northern Peninsular Ranges batholith. Contrib Mineral Petrol 92:351–361

Hoernes S, Friedrichsen H (1980) Oxygen and hydrogen isotopic composition of Alpine and pre-Alpine minerals of the Swiss Central Alps. Contrib Mineral Petrol 72:19–32

James DE (1981) The combined use of oxygen and radiogenic isotopes as indicators of crustal contamination. Ann Rev Earth Planet Sci 9:311–344

Juteau M, Michard A, Albarede F (1986) The Pb–Sr–Nd isotope geochemistry of some recent circum-Mediterranean granites. Contrib Mineral Petrol 92:331–340

Kagami H, Fischer H, Steiger RH (1985) Nd and Sr isotope evidence for the crustal origin of the Periadriatic plutons (abstr). Terra Cognita 5:324

Kagami H, Ulmer P, Hansmann W, Dietrich V, Steiger RH (1991) Nd–Sr isotopic and geochemical characteristics of the southern Adamello (N Italy) intrusives: implications for crustal versus mantle origin. J Geoph Res 96:B14331–14346

Köppel V, Grünenfelder M (1975) Concordant U–Pb ages of monazite and xenotime from the Central Alps and the timing of the high temperature Alpine metamorphism, a preliminary report. Schweiz Mineral Petrogr Mitt 55:129–132

Krogh TE (1973) A low-contamination method for hydrothermal decomposition of zircon and extraction of U and Pb for isotopic age determinations. Geochim Cosmochim Acta 37:485–494

Kyser TK (1990) Stable isotopes in the continental lithospheric mantle. In: Menzies MA (ed) Continental Mantle. Clarendon Press, Oxford

Liew TC, Hoffmann AW (1988) Precambrian crustal components, plutonic associations, plate environment of the Hercynian Fold Belt of central Europe: Indications from a Nd and Sr isotopic study. Contrib Mineral Petrol 98:129–138

Mottana A, Morten L, Brunfelt AO (1978) Distribuzione delle terre rare nel massiccio Val Masino – Val Bregaglia (Alpi Centrali). Rend Soc Ital Mineral Petrol 34:485–497

Nievergelt P, Dietrich V (1977) Die andesitisch-basaltischen Gänge des Piz Lizun (Bergell). Schweiz Mineral Petrogr Mitt 57:267–280

Reusser E (1987) Phasenbeziehungen im Tonalit der Bergeller Intrusion (Graubünden, Schweiz/Provinz Sondrio, Italien). PhD Dissertation, ETH-Zürich

Staub R (1918) Geologische Beobachtungen am Bergeller Massiv. Vierteljahrssch Naturforsch Ges Zürich 63:1–18

Staub R (1921) Geologische Karte der Val Bregaglia (Bergell). Geologische Spezialkarten der Schweiz, Blatt 90

Stern CR, Frey FA, Futa K, Zartman RE, Peng Z, Kyser TK (1990) Trace-element and Sr, Nd, Pb, and O isotopic composition of Pliocene and Quarternary alkali basalts of the Patagonian Plateau lavas of southernmost South America. Contrib Mineral Petrol 104:294–308

Stille P (1987) Geochemische Aspekte der Krustenevolution im zentral- und südalpinen Raum. Habilitationsschrift, ETH Zürich

Stille P, Buletti M (1987) Nd–Sr isotopic characteristics of the Lugano volcanic rocks and constraints on the continental crust formation in the South Alpine domain (N-Italy-Switzerland). Contrib Mineral Petrol 96:140–150

Stille P, Fischer H (1990) Secular variation in the isotopic composition of Nd in Tethys seawater. Geochim Cosmochim Acta 54:3139–3145

Stille P, Steiger RH (1991) Hf isotope systematics in granitoids from the central and southern Alps. Contrib Mineral Petrol 107:273–278

Stille P, Oberhänsli R, Wenger-Schenk K (1989) Hf–Nd isotopic and trace element constraints on the genesis of alkaline and calc-alkaline lamprophyres. Earth Planet Sci Lett 96:209–219

Taylor HP Jr (1980) The effects of assimilation of country rocks by magmas on $^{18}O/^{16}O$ and $^{87}Sr/^{86}Sr$ systematics in igneous rocks. Earth Planet Sci Lett 47:243–254

Tilton GR, Schreyer W, Schertl H-P (1989) Pb–Sr–Nd isotopic behavior of deeply subducted crustal rocks from the Dora Maira Massif, Western Alps, Italy. Geochim Cosmochim Acta 53:1391–1400

Trommsdorff V, Nievergelt P (1983) The Bregaglia (Bergell) Iorio intrusive and its field relations. Mem Soc Geol Italy 26:55–68

Turpin L, Velde D, Pinte G (1988) Geochemical comparison between minettes and kersantites from the Western European Hercynian orogen: trace element and Pb–Sr–Nd isotope constraints on their origin. Earth Planet Sci Lett 87:73–86

Ulmer P (1988) High pressure phase equilibria of a calc-alkaline picro-basalt: Implications for the genesis of calc-alkaline magmas. Carnegie Inst Washington, Ann Rep of the Dir Geoph Lab 2102:28–35

Ulmer P, Callegari E, Sondereggen UC (1983) Genesis of the mafic and ultramafic rocks and their genetical relations to the tonalitic-trondhjemitic granitoids of the southern part of the Adamello batholith (Northern Italy). Mem Soc Geol Ital 26:171–222

Voshage H, Hofmann AW, Mazzucchelli M, Rivalenti G, Sinigoi S, Raczek I, Demarchi G (1990) Isotopic evidence from the Ivrea Zone for a hybrid lower crust formed by magmatic underplating. Nature 347:731–736

Wasserburg GJ, Jacobsen SB, DePaolo DJ, McCulloch MT, Wen T (1981) Precise determination of Sm/Nd ratios, Sm and Nd isotopic abundances in standard solutions. Geochim Cosmochim Acta 45:2311–2323

Weber J (1957) Petrographische und geologische Untersuchung des Tonalitzuges von Melirolo-Sorico zwischen Tessintal und Comersee. Schweiz Mineral Petrogr Mitt 37:267–397

Wedepohl KH (1978) Handbook of geochemistry, vol 2/4. Springer, Berlin Heidelberg New York

Wenk HR (1982) A geological history of Bergell granite and related rocks. In: Drescher-Kaden FK, Augustithis SS (eds): Transformists' Petrology. Theophrastus Publications, Athens, pp 113–148

Wenk HR, Cornelius SB (1977) Geologischer Atlas der Schweiz 1:25000, Blatt 70, Sciora. Schweiz Geol Komm

Wyllie PJ, Wuu-Liang Huang, Stern CR, Maaløe S (1976) Granitic magmas: possible and impossible sources, water contents, and crystallization sequences. Can J Earth Sci 13:1007–1019

Wilson M, Downes H (1991) Tertiary-Quaternary extension-related alkaline magmatism in Western and Central Europe. J Petrol 32:811–849

Yeh H (1980) D/H ratios and late-stage dehydration of shales during burial. Geochim Cosmochim Acta 44:341–352

Editorial responsibility: V. Trommsdorff